IEEE Photonics Journal
An IEEE Photonics Society Publication

Open Access

Free-Space Communication Turbulence Compensation by Optical Phase Conjugation

Volume 12, Number 5, October 2020

Junfan Chen
Yang Huang
Rujun Cai
Anrui Zheng
Zhaoxin Yu
Tianshu Wang
Zhi Liu
Shiming Gao

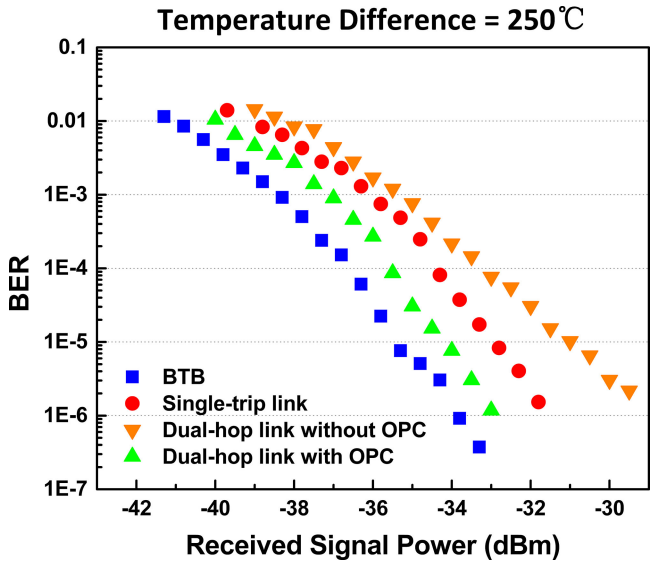

DOI: 10.1109/JPHOT.2020.3024220

Free-Space Communication Turbulence Compensation by Optical Phase Conjugation

Junfan Chen,[1,2] **Yang Huang,**[1,2] **Rujun Cai,**[1,2] **Anrui Zheng,**[1,2] **Zhaoxin Yu,**[1,2] **Tianshu Wang**[3] **, Zhi Liu,**[3] **and Shiming Gao**[1,2]

[1]Center for Optical and Electromagnetic Research, State Key Laboratory of Modern Optical Instrumentation, International Research Center for Advanced Photonics, Zhejiang University, Hangzhou 310058, China
[2]Ningbo Research Institute, Zhejiang University, Ningbo 315100, China
[3]National and Local Joint Engineering Research Center of Space Optoelectronics Technology, Changchun University of Science and Technology, Changchun 130022, China

DOI:10.1109/JPHOT.2020.3024220

Manuscript received August 21, 2020; revised September 4, 2020; accepted September 11, 2020. Date of publication September 15, 2020; date of current version October 2, 2020. This work was supported in part by the National Natural Science Foundation of China under Grant 61875172, in part by the Zhejiang Provincial Natural Science Foundation of China under Grant LD19F050001, and in part by the Fundamental Research Funds for the Central Universities. Corresponding author: Shiming Gao (e-mail: gaosm@zju.edu.cn).

Abstract: A new scheme is proposed to mitigate the atmospheric turbulence effect in coherent free-space optical (FSO) communications by employing optical phase conjugation (OPC) to compensate the signal distortion. The compensation performance of the dual-hop FSO transmission link is simulated using the phase screen method for quadrature phase-shift keying (QPSK) signals. The results show that the bite error rate (BER) can be effectively reduced and the OPC correction is tightly affected by the OPC receiving aperture in strong turbulence regimes. The dual-hop FSO link with the OPC correction is experimentally demonstrated in a turbulence-tunable atmospheric cell, where the OPC is achieved by using degenerate four-wave mixing (DFWM) in a 110-m-long highly nonlinear fiber. At the BER of 1×10^{-3}, the power penalty for dual-hop link with OPC correction decreases about 1.2 dB and 2 dB compared with the single-trip link and the non-compensation dual-hop link. The result demonstrates that the OPC unit can improve the performances of the coherent FSO communication, and it has the potential to be extended to higher-order modulation formats and higher bit rate processing.

Index Terms: Free-space optical communications, four-wave mixing, optical phase conjugation, atmospheric turbulence compensation.

1. Introduction

Free-space optical (FSO) communications take many advantages over traditional microwave systems for their high modulation bandwidth, free license spectrum and enhanced security [1], [2]. The increasing demands for high data rate and large communication capacity in space technology open a new chapter for FSO communication to build ground-to-satellite/satellite-to-ground links, inter-satellite links, and deep space links [3]. Besides, they are considered as one of the mostly technologies for solving the last-kilometer bottle neck in future access networks [4]. Recently, coherent FSO communication systems have been paid more attentions in comparison to common

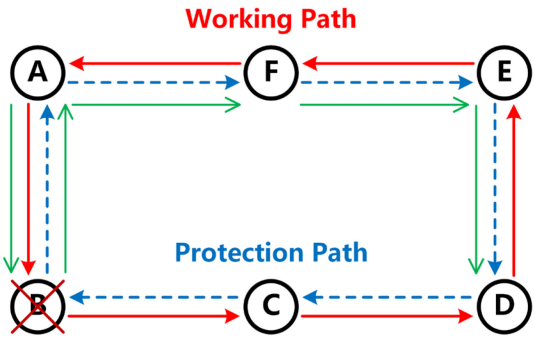

Fig. 1. Mesh topology of FSO ring network with path-switched protection ring. The red solid and blue dashed lines represent the working path and the protection path respectively while the green line represents the path traffic transmitted when node B suddenly fails.

non-coherent intensity modulation/direct detection (IM/DD) schemes, due to their higher sensitivity, longer relay distance, larger communication capacity, and better receiver selectivity [5]. However, the influence of the atmospheric turbulence onto the propagating laser beam can seriously affect the performance of coherent FSO systems, leading to the degradation in bit error rate (BER) and make the communication link infeasible.

In order to reduce the effect of atmospheric turbulences, variety of mitigation techniques have been proposed including aperture averaging technique [6], diversity technique [7], advanced modulation scheme [8], and adaptive optics [3]. Moreover, adaptive optics (AO) are commonly used to compensate for the turbulence-induced wavefront phase aberrations in coherent FSO communication link [9]. The performance improvement of the atmospheric coherent FSO communications using the AO system has been demonstrated theoretically and experimentally verified for satellite-to-ground coherent optical communications [10]–[13]. Though a significant success has been achieved, these approaches based on AO technology revealed some limitations, such as application of highly complicated computation and structures, rather moderate response time (its typical value is about 10^{-3}–10^{-2} sec) and moderate range of spatial frequencies of the distortions (about 200-400 actuators across the adaptive mirror). In comparison, due to the all optical phase conjugation (OPC) techniques, the compensations based on OPC for atmospheric turbulences have much shorter response time (10^{-9}–10^{-7} sec) and less limitations of the affordable spatial frequencies [14]. The aberration influence imposed on the forward beam that passes through the atmospheric turbulence can be automatically removed for the backward OPC beam that passes through the same one. It can provide in principle a significant gain in the energy delivered to the remote receiver and greatly improve the performance of the FSO system over strong turbulences.

OPC can be realized based on stimulated emission, various simulated scatterings (Brillouin, Raman, Rayleigh-wing or Kerr scattering), three-wave mixing in a second-order nonlinear medium, or degenerate four-wave mixing (DFWM) in a third-order nonlinear medium [15]. In the past, a number of works focused on different technical approaches to produce phase conjugate beam and the ability to correct for beam distortions [16]–[19]. However, to our best knowledge, the application of the OPC technique on the coherent FSO link to compensate for the turbulence-induced phase aberrations and decrease the degradation of the signal has not yet been reported.

A self-healing ring is often adopted to mitigate network component failures in ring network architectures [20], [21]. The dual-hop link with the OPC technique can be applied to the FSO self-healing ring network as a part of protection scheme. As depicted in Fig. 1, the traffic is transmitted simultaneously on the working path from node A to node D through link A-B-C-D. If node B fails, it can switch the traffic to the protection path and the traffic will back to node A while the phase conjugation technique can remove the distortions and ensure the operation of the protection path. In such a system, dual-hop FSO links play an important role to ensure the system available.

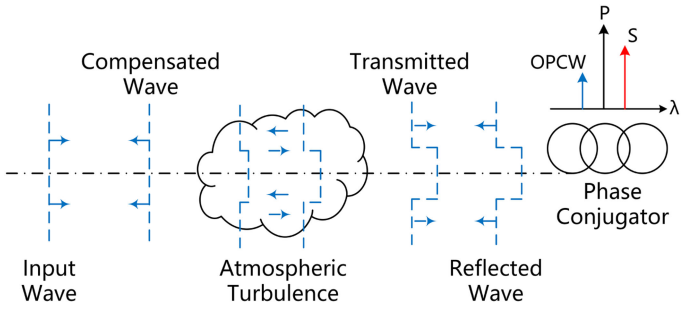

Fig. 2. Schematic diagram of turbulence mitigation for the dual-hop FSO link with OPC correction. When the OPCW backward passes through the turbulence, the aberration influence is compensated.

In this paper, a novel coherent dual-hop FSO link with the OPC unit to compensate the turbulence distortion is proposed and demonstrated. The performance of the OPC correction is evaluated by numerical simulations and experiments. In section 2, the theoretical model of the turbulence mitigation by OPC is established, which indicates that the distortion influence imposed on the transmitted wave through the atmospheric turbulence can be removed for the backward OPC wave (OPCW) that passes through the same atmospheric turbulence. In section 3, we simulate the atmospheric channel to analyze the performance improvement of the coherent dual-hop link with OPC correction. In section 4, the experiment of the dual-hop FSO link with the OPC correction system is carried out and the link improvement of the OPC correction is demonstrated by measuring the scintillation index of the received power and the BER of the link. Finally, the conclusion is drawn in section 5.

2. Principles of the Turbulence Corrected Method

Fig. 2 illustrates the principle of the turbulence mitigation for the dual-hop FSO link with OPC. The phase of the laser beam transmitted in the atmospheric turbulence will be distorted, resulting in a random deviation of the propagation direction, the beam spread, and the far-field intensity distribution modulation. Suppose the incident wave is an ideal plane-monochromatic wave, and after passing through the atmospheric turbulence it can be expressed by

$$\boldsymbol{E}\,(z,x,y,\omega)=\boldsymbol{E}\,(z,x,y)\,e^{-i\omega t}=\boldsymbol{A}_0\,(z,x,y)\,e^{i[kz+\varphi(z,x,y)]}e^{-i\omega t} \tag{1}$$

Here, z is the longitudinal variable along the propagation direction, x and y are the radial variables along the beam section, ω is the circular frequency of the incident field, k is the wavenumber, $\boldsymbol{E}(z,x,y)$ is the complex amplitude function, and $\boldsymbol{A}_0(z,x,y)$ is the real amplitude function. $\varphi(z,x,y)$ is a phase function describing the aberration influence of the turbulence on the wavefront.

And then, the OPCW is generated through DFWM in a highly nonlinear fiber (HNLF), which is pumped by a continuous-wave light with a small frequency difference compared to the transmitted wave. The forward-propagated OPCW is supported to meet the requirement for minimum phase mismatching. Therefore, the OPCW can be written as:

$$\boldsymbol{E'}\left(z,x,y,\omega'\right)=\bar{R}\cdot\boldsymbol{E^*}\,(z,x,y)\,e^{-i\omega' t}=\bar{R}\cdot\boldsymbol{A}_0\;(z,x,y)\,\mathrm{e}^{-i[k'z+\varphi'(z,x,y)]}\mathrm{e}^{-i\omega' t} \tag{2}$$

where $\omega'=2\omega_{pump}-\omega$, and $\bar{R}$ is the effective amplitude reflectivity of the phase conjugator. When the frequency of the incident field (ω) is not equal to the pump frequency (ω_{pump}), the OPCW will have a frequency of ($2\omega_{pump}-\omega$), which is slightly shifted from the incident signal. After passing back through the same turbulence the output wave will be

$$\boldsymbol{E''}\left(z,x,y,\omega'\right)=\bar{R}\cdot\boldsymbol{A}_0\;(z,x,y)\,e^{-i[k'z+\varphi'(z,x,y)]}e^{i\varphi(z,x,y)}e^{-i\omega' t}=\bar{R}\cdot\boldsymbol{A}_0\;(z,x,y)\,e^{-ik'z}e^{-i[\Delta\varphi(z,x,y)]}e^{-i\omega' t} \tag{3}$$

where $\Delta\varphi\;(z,x,y)=\varphi'\;(z,x,y)-\varphi(z,x,y)$. If the wavelength difference between the OPCW and the incident wave is small enough, the phase difference $\Delta\varphi$ can be regarded as near-zero. One

can see an ideal output plane wave without any aberration influence from the turbulence can be obtained, which means that the turbulence distortion is corrected by OPC. In fact, the compensation will be imperfect because of the dynamic of the atmospheric channel and the wavelength difference of the OPCW. Besides, it will also be affected by the loss of high spatial frequency components of the incident distorted light due to the limited aperture of the optical antenna while the light with large angular divergence cannot be fully collected [17].

To evaluate the influence of atmospheric turbulence imposed on the laser beam, the phase distortions can be physically modelled and numerically simulated by using the phase screen method [7]. The total propagation distance is sectioned into smaller turbulent layers, and each layer is considered as a unit-amplitude thin phase screen. In each segment, the linear propagation processes are performed in the spatial frequency domain or k-space, whereas the nonlinearities and random processes caused by atmospheric turbulence are carried out in the space domain $(x,\ y)$. Turbulent simulations can be performed by superimposing several phase screens under the condition of specifying the distribution of the incident optical field [22].

The profile $\boldsymbol{E}(z, x, y)$ at an arbitrary plane z is Fourier transformed, and the angular plane wave spectrum is multiplied by the propagation function in the spatial frequency domain $(k_x,\ k_y)$, to incorporate the effects of diffraction:

$$\tilde{\boldsymbol{E}}\left(z+\Delta z,\ k_x,\ k_y\right)=\mathcal{F}\left[\boldsymbol{E}\left(z,x,y\right)\right]e^{\frac{i\left(k_x^2+k_y^2\right)\Delta z}{2k_0}} \tag{4}$$

The inverse Fourier transform returns the spectrum to the space domain, where the phase change caused by the qth phase screen is multiplied:

$$\boldsymbol{E}\left(z+\Delta z,x,y\right)=\mathcal{F}^{-1}\left\{\tilde{\boldsymbol{E}}\left(z+\Delta z,\ k_x,\ k_y\right)\right\}\phi_q\left(\Delta z,x,y\right) \tag{5}$$

The process is repeated for each slice in the total propagation distance. To generate phase screens on a finite grid, the phase screen can be written as a Fourier series [23]:

$$\phi_q\left(\Delta z,x,y\right)=\sum_{n=-\infty}^{\infty}\sum_{m=-\infty}^{\infty}c_{n,m}\exp\left[i2\pi\left(f_{x_n}x+f_{y_m}y\right)\right] \tag{6}$$

where f_{x_n} and f_{y_m} are the discrete x- and y-directed spatial frequencies, and the $c_{n,m}$ are the Fourier-series coefficients. In general, the real and imaginary parts of $c_{n,m}$ have zero means and follow a Gaussian distribution, of which the variance given by

$$\left\langle\left|c_{n,m}\right|^2\right\rangle=\Phi_\phi\ \left(f_{x_n},f_{y_m}\right)\Delta f_{x_n}\Delta f_{y_m} \tag{7}$$

where Δf_{x_n} and Δf_{y_m} represent the frequency spacings, and $\Phi_\phi(f_{x_n}, f_{y_m})$ is the spatial power spectral density. Converting f_{x_n} and f_{y_m} to θ and f in polar coordinates, the modified von Karman spectrum model is used to describe the phase screen statistics as [24]

$$\Phi_\phi\left(k\right)=\frac{0.33C_n^2}{\left(k^2+k_0^2\right)^{11/6}}\ e^{-\left(\frac{k^2}{k_m^2}\right)} \tag{8}$$

where k is the spatial wavenumber, $k_m=5.92/l_0$, $k_0=2\pi/L_0$. C_n^2 is the atmospheric refraction-index structure parameter, L_0 and l_0 are the outer and inner scales of the turbulence, respectively.

3. Numerical Simulations and Discussion

In numerical simulations, the laser carrier is set as a Gaussian beam and the simulation parameters are as follow: the wavelength of the incident signal beam is 1550.1 nm while the wavelength of the backward phase conjugate beam is 1546.9 nm, the propagation distance L is 1 km, which is divided into 10 segments with each interval of 100 m and the phase screen is set in the middle of each segment, the outer scale of turbulence L_0 and inner scale of turbulence l_0 are 100 m and 0, respectively. The strengths of the atmospheric turbulence are described by the atmospheric

TABLE 1
The C_n^2 Values Corresponding to Weak, Moderate, and Strong Turbulences

	Weak	Moderate	Strong
Value Range ($\mathrm{m}^{-2/3}$)	$< 1 \times 10^{-14}$	$1 \times 10^{-14} \sim 1 \times 10^{-13}$	$> 1 \times 10^{-13}$

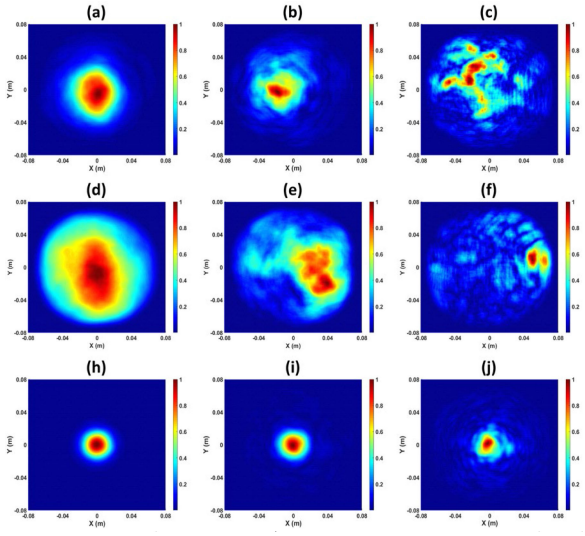

Fig. 3. Simulated normalized optical fields at the receiver when $C_n^2 = 2 \times 10^{-15}$, 3×10^{-14}, and 3.2×10^{-13} $\mathrm{m}^{-2/3}$ (corresponding to $\sigma_R^2 =$ 0.0398, 0.597 and 6.37). (a)–(c) are for the single-trip link, (d)–(f) are for the dual-hop link without OPC correction, and (h)–(j) are for the dual-hop link with OPC correction.

refraction-index structure parameter C_n^2 and the Rytov variance $\sigma_R^2 = 1.23k^{7/6}C_n^2L^{11/6}$ (here k is the wavenumber and L is the propagation distance). Here, we divide the condition of turbulence into weak, moderate and strong turbulences (illustrated in Table 1) [24]. When the size of receiving aperture (D) takes the value of 0.16 m, Fig. 3 shows the normalized optical field distributions when the signal beam transmits in the atmospheric channel. As shown in Fig. 3(a)–(c), the beam energy concentration is obviously impacted by the atmospheric turbulence in the single-trip FSO link, and higher diffusion and distortion of the optical field occurs when the turbulence gets stronger. The distortion accumulates and the signal optical field gets worse after dual-hop FSO transmission, as shown in Fig. 3(d)–(f). However, in the dual-hop FSO link with the OPC correction, the beam pattern at the reception plane shows a shape of almost ideal diffraction spot under weak and moderate turbulences, which means that the atmospheric distortion is almost entirely compensated. With the strong turbulence, the diffusion of the optical field is much less than it with the single-trip link and the non-compensation dual-hop link.

The beam distortion results in the variation of the signal power and the shift of the signal phase, degrading the BER performance. In order to quantitatively analyze the performance of the OPC compensation, the BER of the dual-hop link with OPC correction is simulated (based on the work reported in [7] and [24]), and the BERs of the single-trip and non-compensation dual-hop FSO links are also simulated for comparison, as depicted in Figs. 4. Considering a 5 Gbit/s quadrature phase-shift keying (QPSK) signal, the signal passing through the turbulent channel is simulated based on "frozen turbulence" hypothesis [7]. The simulation is performed with different C_n^2 containing weak, moderate and strong turbulences. Under different parameters conditions, 100 sets of data are recorded with the length of 1×10^6 symbols to calculate the BER respectively, and then to calculate the average BER. Simulation was optimized using data from experimental

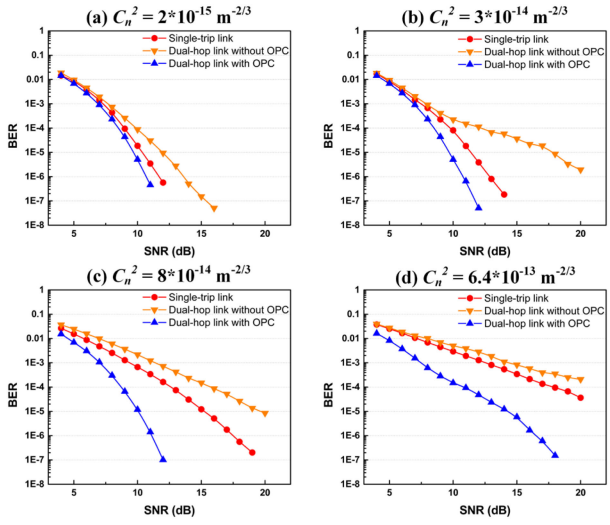

Fig. 4. Simulated BERs of the coherent dual-hop link with OPC correction compared with single-trip link and non-compensation dual-hop link when (a) C_n^2 takes the value of 2×10^{-15} m$^{-2/3}$, (b) C_n^2 takes the value of 3×10^{-14} m$^{-2/3}$, (c) C_n^2 takes the value of 8×10^{-14} m$^{-2/3}$, and (d) C_n^2 takes the value of 6.4×10^{-13} m$^{-2/3}$.

measurements and then was used for the simulation of the FSO link. Comparing the results of the single-trip link and dual-hop links, it can be seen that the reception performance can be effectively improved by introducing OPC correction. As shown in Fig. 4(a), at the signal-to-noise ratio (SNR) of 11 dB and with relatively weak turbulence ($C_n^2 = 2 \times 10^{-15}$ m$^{-2/3}$), the BER of dual-hop link with OPC correction is 4.56×10^{-7}, which is two orders of magnitude lower than the BER of the non-compensation dual-hop link. The improvement for moderate atmospheric turbulence is more remarkable [see Fig. 4(b) and (c)]. The BERs reduce from 1.63×10^{-4} with the single-trip link and 7.24×10^{-4} with the non-compensation dual-hop link to 1.01×10^{-7} after the OPC compensation with $C_n^2 = 8 \times 10^{-14}$ m$^{-2/3}$ at an SNR of 12 dB. Under weak and moderate turbulences, almost full compensation of atmospheric distortions can be attained. However, under the strong turbulence, as shown in Fig. 4(d), the BERs evidently go up for SNR higher than 9 dB compared to others, which indicates that the severe signal drift and degradation caused by the atmospheric turbulence is difficult to be fully compensated.

Furthermore, the quantitative characteristics of the OPC correction versus the size of receiving aperture at the OPC terminal in different turbulence regimes are discussed in Fig. 5. When the refraction-index structure parameters C_n^2 are 8×10^{-15} and 8×10^{-14} m$^{-2/3}$, corresponding to weak and moderate turbulences, one can find that the BER performances are almost insensitive to the aperture diameter once the diameter is larger than 0.16 m. The reason is that the signal beam distortion is slight and it can be easily collected. Under the strong turbulences ($C_n^2 = 4 \times 10^{-13}$ and 8×10^{-13} m$^{-2/3}$), the BERs are obviously improved with the expansion of the receiving aperture. For the two kinds of turbulences, the minimum aperture diameters of $D = 0.22$ m and $D = 0.26$ m are required to almost fully compensate the atmospheric distortions, since the increase of the aperture size enlarges the cutoff spatial frequency and helps to enhance the fidelity of OPC correction when the signal beam is greatly distorted in strong turbulences.

4. Experimental Setup and Results

Fig. 6 shows the experimental setup of the OPC-corrected dual-hop coherent FSO communication link. The optical carrier emitted from a DFB laser (with a wavelength of 1550.1 nm and linewidth ~35 kHz) is modulated by a 5 Gbit/s QPSK sequences generated by 2^{15}–1 pseudo-random

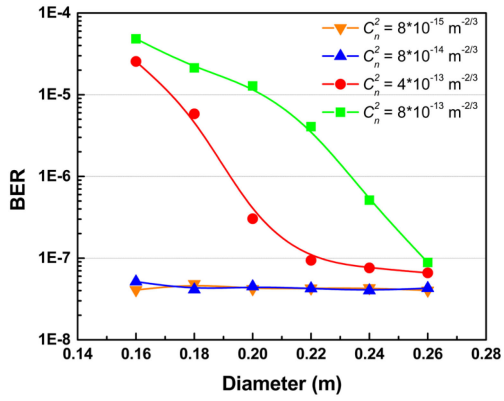

Fig. 5. Simulated BERs of the coherent dual-hop FSO link with OPC correction versus the diameter of aperture (D) at the SNR of 12 dB when C_n^2 takes the values of 8×10^{-15}, 8×10^{-14}, 4×10^{-13}, and 8×10^{-13} m$^{-2/3}$.

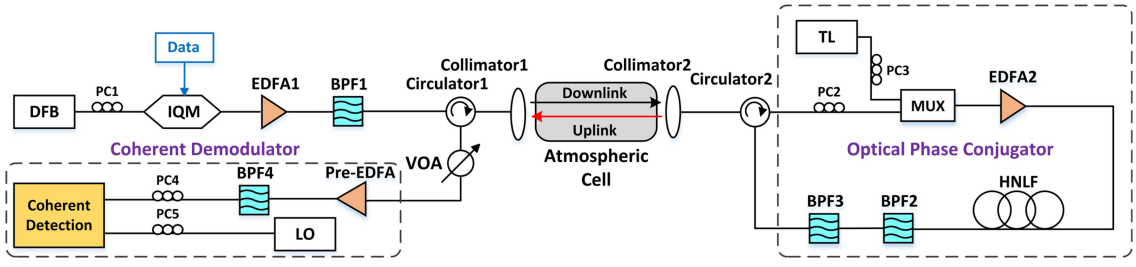

Fig. 6. Experimental setup of the dual-hop FSO communication link with OPC correction.

bit sequence (PRBS) from the signal generator through an in-phase quadrature (IQ) modulator (Fujitsu FTM7962). It is amplified to 13 dBm by an erbium-doped fiber amplifier (EDFA, Amonics AEDFA-13) and transmitted into the atmospheric cell through circulator 1 and collimator 1 (Thorlabs F810FC-1550). The focal length of the collimator f = 37.13 mm and the numerical aperture NA = 0.24. After propagation, the distorted signal is injected into the OPC unit after being collected by collimator 2 (the same as collimator 1).

The OPC is based on DFWM pumped by a tunable laser with a wavelength of 1548.5 nm. The distorted signal is combined with the pump by a multiplexer (MUX) and amplified using an EDFA to the total output power of 23 dBm before launching into the 110-m-long HNLF, where DFWM occurs to generate the OPCW. The polarization states of the QPSK signal and the pump are both aligned to each other by adjusting the polarization controllers (PC2 and PC3). Fig. 7 shows the measured optical spectrum of the OPCW generation using an optical spectrum analyzer (YOKOGAWA AQ6370D). The converted OPCW is switched to the wavelength of 1546.9 nm and the power is measured to be −0.3 dBm, corresponding to the conversion efficiency of −17.1 dB.

The generated OPCW is filtered by two 0.8-nm bandpass filters (BPF2 and BPF3), and then transmitted backward via circulator 2 and collimator 2 once more. After the propagation in the atmospheric cell, the QPSK signal is filtered and pre-amplified by a pre-EDFA while a variable optical attenuator (VOA) is applied to change the optical power of the received signal for performance measurement. Digital coherent detection is used to convert the complicated phase information to the digital domain and demodulated.

The propagation path used in the experiment is established in a 1.5-m-long atmospheric cell by introducing a temperature difference between its top and bottom. As the temperature difference increasing, the turbulence will become stronger while the temperature difference can raise up to

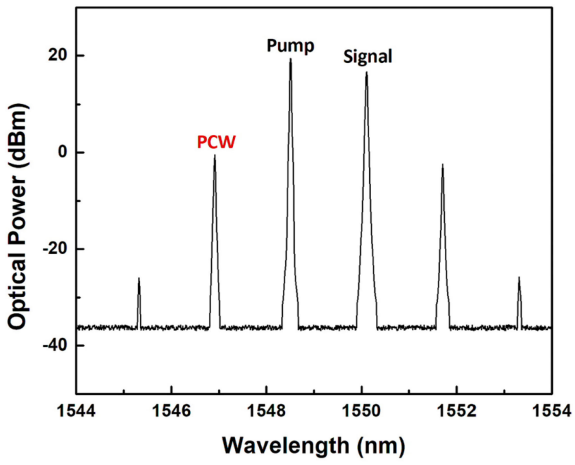

Fig. 7. Measured optical spectrum of the OPCW generation process with a resolution of 0.05 nm.

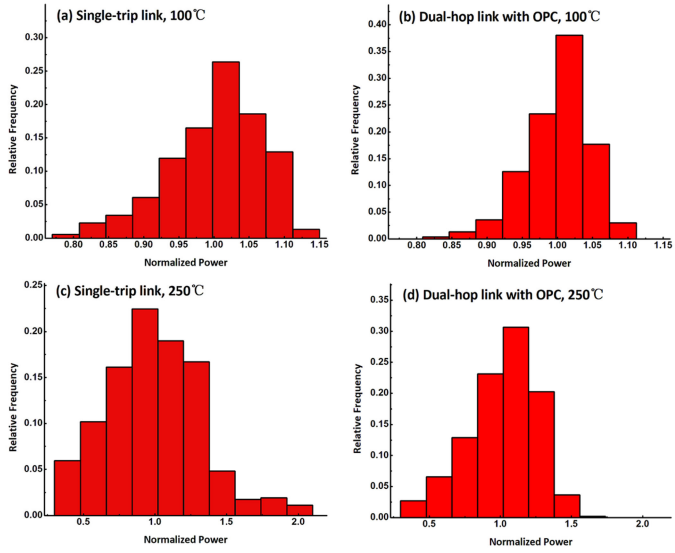

Fig. 8. Measured relative frequency distributions of the received power for the single-trip link and the dual-hop link with OPC correction. (a) and (b) are at temperature difference of 100 °C, while (c) and (d) are at temperature difference of 250 °C.

250 °C in the maximum extent. Due to the limitation of the temperature difference, the atmospheric cell can only simulate weak turbulence condition. To evaluate the influence of the atmospheric turbulence on optical signal, the scintillation index as well as Rytov variances were calculated in Ref. [25]. We present the Rytov variances for two different temperature difference, i.e., 0.0062 for 100 °C and 0.1231 for 250 °C, corresponding to C_n^2 of 3.11×10^{-16} and 6.18×10^{-15} $m^{-2/3}$ in a 1-km-long outdoor atmospheric channel. The turbulence experienced by the downlink signal is correlated to the uplink due to the negligible time interval. The optical power attenuation of the downlink is ~13.5 dB, similar to the uplink, owing to the propagation losses and the coupling losses from free-space to fibers.

The fluctuation of the received power is measured for the dual-hop FSO link with the OPC correction together with that for the single-trip FSO link as a comparison. Fig. 8 shows the measured power distributions at different temperature differences of 100 and 250 °C, respectively.

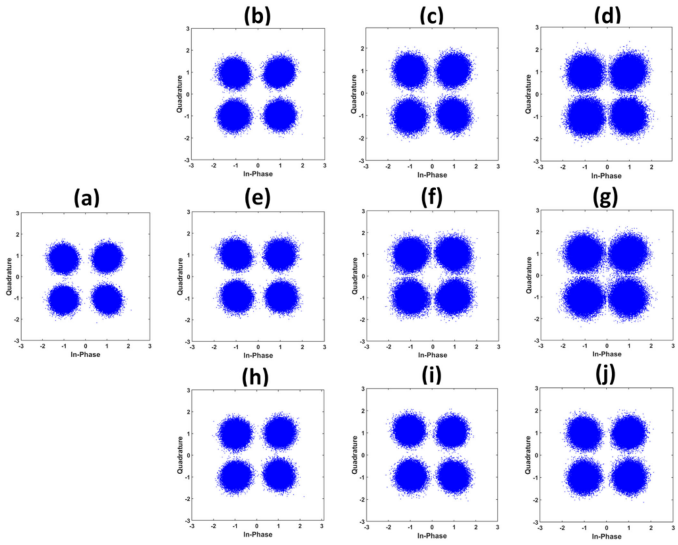

Fig. 9. Measured constellation diagrams of (a) the BTB signal, the single-trip link transmission signals with the temperature differences of (b) 0 °C, (c) 100 °C, (d) 250 °C, the non-compensation dual-hop link transmission signals with the temperature differences of (e) 0 °C, (f) 100 °C, (g) 250 °C, and the OPC-compensated dual-hop link transmission signals with the temperature differences of (h) 0 °C, (i) 100 °C, and (j) 250 °C.

The scintillation indexes of the optical power are 0.0020 and 0.0055 in the case of the dual-hop link with OPC and the single-trip link at temperature difference of 100 °C. As the temperature difference reach 250 °C, they increase to 0.059 and 0.116, respectively. The scintillation indexes are measured as the variance of the received power normalized by the square of the average [26]. With the increase of the temperature difference, the optical power deviation from the average is getting larger due to the aggravation of the atmospheric turbulence. The power deviation of the dual-hop link with OPC is less than the single-trip link. When the OPC unit is on, the power fluctuations can be effectively reduced. However, it is seen that the improvement is not crucial owing to the relatively weak turbulence.

Fig. 9 shows the constellation diagrams for the back-to-back (BTB), the single-trip link, the non-compensation dual-hop link, and the compensated dual-hop link when the received signal power are fixed at -35 dBm with the temperature differences of 0, 100 and 250 °C, respectively. The root-mean-square error vector magnitude of the single-trip link and the two dual-hop links are calculated as 0.4027, 0.4221, and 0.3439 at temperature difference of 250 °C, while it is 0.3334 for the BTB case. The phase fluctuation of the signal transmitted by the dual-hop link with OPC only increases a little compared to the original signal. With the temperature difference increasing, the qualities of constellation diagram degrade for the single-trip link and non-compensation dual-hop link, however, the fading of constellation diagram for the dual-hop link with OPC is much less, which represent a considerable improvement by using OPC.

Fig. 10 shows the BER performances of the FSO transmission measured with the 5 Gbit/s QPSK signal. As shown in Fig. 10(a), under the temperature difference of 0 °C, the atmospheric turbulence is too weak to affect the FSO transmission, so that the curves for the BTB, the single-trip link, the dual-hop links without and with OPC all almost stick together as the received signal power varies. When the temperature difference is 100 °C [see Fig. 10(b)], at the BER of 1×10^{-3}, the power penalty for the dual-hop link with OPC is obtained to be 0.6 dB, decreasing about 0.3 dB compared with that for the single-trip link and 0.8 dB for the non-compensation dual-hop link, while the improvements raise up to 1.2 dB and 2 dB for 250 °C. Considering the received power of -33.5 dBm at the temperature difference of 250 °C, as shown in Fig. 10(c), the BER reduces by two magnitude orders as 3.05×10^{-6} for the dual-hop link with OPC correction and 1.45×10^{-4} for

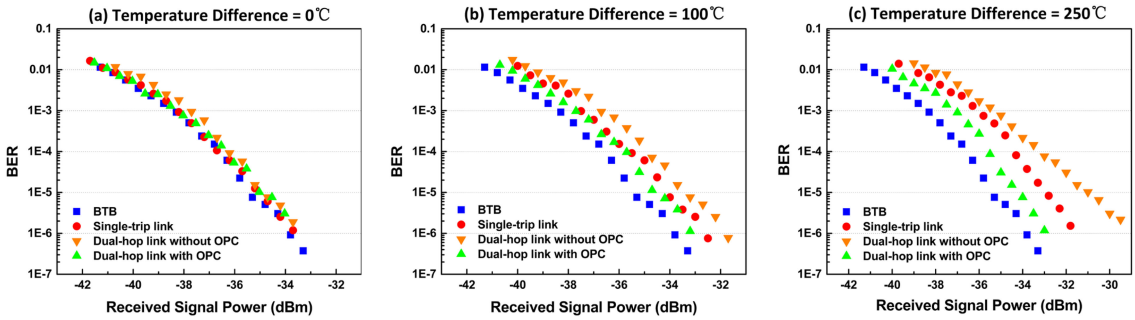

Fig. 10. Measured BER performance as a function of the received power for the BTB, the single-trip link, the dual-hop link without OPC, and the dual-hop link with OPC when the temperature differences are (a) 0 °C, (b) 100 °C, and (c) 250 °C, respectively.

the dual-hop link without OPC. A considerable improvement can be achieved with OPC correction as the signal is moderately suffered by the turbulence, and the compensation by OPC unit will be more prominent with the turbulence getting stronger. In our experiment, a 5 Gbit/s QPSK signal is used due to the limitation of the equipment. In principle, our proposed dual-hop FSO link with OPC correction can support higher-order modulation formats and higher modulation bit rate.

5. Conclusion

A coherent dual-hop FSO link with OPC correction has been proposed and experimentally demonstrated under different turbulence regimes. The OPC compensation performance with the Gaussian beam in the atmospheric channel has been numerically simulated using the phase screen method. The turbulence-induced phase aberrations in the FSO link can be effectively mitigated, especially in the relatively strong turbulence regime. The BER can reduce by three orders of magnitude for the moderate turbulence of $C_n^2 = 8 \times 10^{-14}$ m$^{-2/3}$ at an SNR of 12 dB. Moreover, the quality of OPC correction can be further improved by expanding the aperture size. The experiment of the coherent dual-hop FSO link for 5 Gbit/s QPSK signals is carried out in an atmospheric cell. The scintillation index, the constellation diagram, and the BER are measured. The power penalty for the dual-hop link with OPC correction decreases about 2 dB compared to the non-compensation dual-hop link at the temperature difference of 250 °C. The results show the quality of the signal can be effectively improved by using the OPC unit. The OPC-corrected FSO link can be adopted as a part of protection scheme to mitigate network component failures in ring network architectures. Furthermore, it has shown the potential in the FSO communication networks based on ad hoc topologies to avoid paths that are severely affected by turbulence and decrease the outage probability [27], [28].

References

[1] M. A. Khalighi and M. Uysal, "Survey on free space optical communication: A communication theory perspective," *IEEE Commun. Surv. Tutor.*, vol. 16, no. 4, pp. 2231–2258, Fourthquarter 2014.
[2] V. W. S. Chan, "Free-space optical communications," *J. Lightw. Technol.*, vol. 24, no. 12, pp. 4750–4762, Dec. 2006.
[3] H. Kaushal and G. Kaddoum, "Optical communication in Space: Challenges and mitigation techniques," *IEEE Commun. Surv. Tutor.*, vol. 19, no. 1, pp. 57–96, Firstquarter 2017.
[4] J. Akella, M. Yuksel, and S. Kalyanaraman, "Multi-channel communication in free-space optical networks for the last-mile," in *Proc. LANMAN*, Princeton, NJ, USA, 2007, pp. 43–48.
[5] J. Cao, X. Zhao, W. Liu, and H. Gu, "Performance analysis of a coherent free space optical communication system based on experiment," *Opt. Express*, vol. 25, no. 13, pp. 15299–15312, Jun. 2017.
[6] S. D. Lyke, D. G. Voelz, and M. C. Roggemann, "Probability density of aperture-averaged irradiance fluctuations for long range free space optical communication links," *Appl. Opt.*, vol. 48, no. 33, pp. 6511–6527, 2009.

[7] Z. X. Yu *et al.*, "Performance evaluation of direct-detection coherent receiver array for free-space communications with full-link simulation," *Opt. Commun.*, vol. 454, no. 124520, Jan. 2020.
[8] I. B. Djordjevic, "Adaptive modulation and coding for free-space optical channels," *IEEE/OSA J. Opt. Commun. Netw.*, vol. 2, no. 5, pp. 221–229, May 2010.
[9] C. Yang, C. Xu, W. Ni, Y. Gan, J. Hou, and S. Chen, "Turbulence heterodyne coherent mitigation of orbital angular momentum multiplexing in a free space optical link by auxiliary light," *Opt. Express*, vol. 25, no. 21, pp. 25612–25624, Oct. 2017.
[10] C. Liu, S. Chen, X. Li, and H. Xian, "Performance evaluation of adaptive optics for atmospheric coherent laser communications," *Opt. Express*, vol. 22, no. 13, pp. 15554–15563, Jun. 2014.
[11] W. Liu, K. Yao, D. Huang, X. Lin, L. Wang, and Y. Lv, "Performance evaluation of coherent free space optical communications with a double-stage fast-steering-mirror adaptive optics system depending on the Greenwood frequency," *Opt. Express*, vol. 24, no. 12, pp. 13288–13302, Jun. 2016.
[12] H. Jian, D. Ke, L. Chao, Z. Peng, J. Dagang, and Y. Zhoushi, "Effectiveness of adaptive optics system in satellite-to-ground coherent optical communication," *Opt. Express*, vol. 22, no. 13, pp. 16000–16007, Jun. 2014.
[13] M. Chen, C. Liu, D. Rui, and H. Xian, "Performance verification of adaptive optics for satellite-to-ground coherent optical communications at large zenith angle," *Opt. Express*, vol. 26, no. 4, pp. 4230–4242, Feb. 2018.
[14] N. A. Romanov, A. A. Leshchev, A. Y. Rodionov, V. E. Semenov, V. E. Sherstobitov, and N. V. Vysotina, "Nonlinear phase-conjugate mirrors for atmospheric distortion compensation," in *Laser Material Crystal Growth and Nonlinear Materials and Devices*, San Jose, CA, USA, 1999, pp. 164–175.
[15] G. S. He, "Optical phase conjugation: Principles, techniques, and applications," *Prog. Quantum Electron.*, vol. 26, no. 3, pp. 131–191, May 2002.
[16] V. Wang and C. Giuliano, "Correction of phase aberrations via stimulated Brillouin scattering," *Opt. Lett.*, vol. 2, no. 1, pp. 4–6, Jan. 1978.
[17] P. Lebow and J. Ackerman, "Phase conjugation through Brillouin-enhanced four-wave mixing over an extended atmospheric path," *Opt. Lett.*, vol. 14, no. 4, pp. 236–238, Feb. 1989.
[18] R. Lind and G. Dunning, "Demonstration of real-time compensation of atmospheric turbulence by nonlinear phase conjugation," in *Proc. Conf. Lasers and Electro-Optics*, Baltimore, MD, USA, 1983, p. THC3.
[19] Y. L. Wang, Z. W. Lu, and Y. Li, "Investigation on high power phase compensation of strong aberrations via stimulated Brillouin scattering," *Appl. Phys. B*, no. 99, pp. 257–261, Mar. 2010.
[20] T.-H. Wu and R. C. Lau, "A class of self-healing ring architectures for SONET network applications," *IEEE Trans. Commun.*, vol. 40, no. 11, pp. 1746–1756, Nov. 1992.
[21] N. Nagatsu, A. Watanabe, S. Okamoto, and K. Sato, "Architectural analysis of multiple fiber ring networks employing optical paths," *J. Lightw. Technol.*, vol. 15, no. 10, pp. 1794–1804, Oct. 1997.
[22] E. M. Whitfield, P. P. Banerjee, and J. W. Haus, "Propagation of Gaussian beams through a modified von Karman phase screen," *Laser Communication and Propagation through the Atmosphere and Oceans*, San Diego, CA, USA, 2012, p. 85170P.
[23] J. D. Schmidt, "Propagation through Atmospheric Turbulence," in *Numerical Simulation of Optical Wave Propagation*, Bellingham, WA, USA: SPIE, 2010, ch. 9, pp. 149–184.
[24] L. C. Andrews and R. L. Phillips, *Laser Beam Propagation Through Random Media*, 2nd ed., Bellingham, WA, USA: SPIE, 2005.
[25] X. L. Feng *et al.*, "60 Gbit/s coherent wavelength-division multiplexing free-space optical modulating retro-reflector in a turbulence-tunable atmospheric cell," *Opt. Commun.*, vol. 448, pp. 111–115, May 2019.
[26] L. C. Andrews, R. L. Phillips, and C. Y. Young, *Laser Beam Scintillation with Applications*, Bellingham, WA, USA: SPIE, 2001, p. 67.
[27] J. Libich, M. Komanec, S. Zvanovec, P. Pesek, W. Popoola, and Z. Ghassemlooy, "Experimental verification of an all-optical dual-hop 10 Gbit/s free-space optics link under turbulence regimes," *Opt. Lett.*, vol. 40, no. 3, pp. 391–394, Jan. 2015.
[28] J. Perez, S. Zvanovec, Z. Ghassemlooy, and W. Popoola, "Experimental characterization and mitigation of turbulence induced signal fades within an ad hoc FSO network," *Opt. Express*, vol. 22, no. 3, pp. 3208–3218, Feb. 2014.